1993

Studies of Electron-Beam Penetration and Free-Carrier Generation in Diamond Films

R. P. Joshi
Old Dominion University

K. H. Schoenbach
Old Dominion University

C. Molina
Old Dominion University

W. W. Hofer

Original Publication Citation

Joshi, R. P., Schoenbach, K. H., Molina, C., & Hofer, W. W. (1993). Studies of electron-beam penetration and free-carrier generation in diamond films. *Journal of Applied Physics, 74*(3), 1568-1574. doi:10.1063/1.354829

Studies of electron-beam penetration and free-carrier generation in diamond films

R. P. Joshi, K. H. Schoenbach, and C. Molina
Department of Electrical and Computer Engineering, Old Dominion University, Norfolk, Virginia 23529-0246

W. W. Hofer
Lawrence Livermore National Laboratory, University of California, Livermore, California 94550

(Received 21 December 1992; accepted for publication 17 April 1993)

Experimental observations of the energy-dependent electron-beam penetration in type II-A natural diamond are reported. The experimental data are compared with results obtained from numerical Monte Carlo simulations, and the results are in very good agreement. The results also reveal that a threshold energy of about 125 keV is necessary for complete penetration for a 35 μm sample. It is found that over the 30–180 keV range, the energy dependence of the penetration depth and total path length exhibits a power-law relation. Monte Carlo simulations have also been performed to investigate the excess carrier-generation profiles within diamond for a set of incident *e*-beam energy distributions. The simulation results demonstrate the feasibility of tailoring the internal source function, and hence influencing the diffusion currents, the internal electric fields, and charge injection through the contacts.

I. INTRODUCTION

Interaction of electron beams with solid targets have long been studied for a variety of reasons. Initial investigations were mainly aimed at gaining a fundamental understanding of the elastic and inelastic electronic scattering processes in condensed matter.[1–6] Electron-beam bombardment was also of interest from the standpoint of solid-state particle detectors,[7] because of the large conductivity variations that could be produced in insulators. More recent applications have focused on using *e* beams as tools for investigating and characterizing material properties of both insulators and semiconductors.[8] Techniques routinely used for such purposes have included electron microscopy, Auger electron spectroscopy, reflection high-energy electron diffraction, and electron energy-loss spectroscopy.

Our current interest in electron beams derives from their potential as efficient ionizing sources for bulk semiconductor-based repetitive closing and opening switches. The development of such repetitive opening switches, capable of carrying large currents and having the potential to hold off large voltages, is critical to pulsed-power technology.[9] The electron beams in this context trigger and independently control the conductivity modulations, provide a less expensive alternative to optical excitation, have higher sustained intensities, and can offer variable duty cycles.[10,11] Other advantages include larger absorption coefficients, wider energy ranges, jitter-free control, electrical isolation, and an inherently fast switching capability. Such *e*-beam-induced switching has already been successfully demonstrated in bulk GaAs (Ref. 11) and polycrystalline diamond.[12] Diamond promises to be a better candidate for switching than GaAs, since it can hold off higher voltages, has shorter carrier lifetime and hence the potential for faster turn-off, exhibits superior thermal conductivity providing for better heat dissipation, has lower dark currents, and is more rugged mechanically. Fortunately, recent advances in processing technology and the successful growth of high-quality artificial diamond[13–15] has made it a viable material. It therefore becomes quite meaningful to investigate electron-beam interactions within thin diamond targets for potential power switching applications.

In this article we report our experimental observations of the energy-dependent electron-beam penetration in natural, type II-A, 35-μm-thick diamond disks. The experimental data are compared with results obtained from numerical Monte Carlo simulations. We find very good agreement between the two, and hence have a high level of confidence in our simulation procedures. The Monte Carlo technique developed here, is also used to investigate the excess carrier-generation profiles within diamond for a set of incident *e*-beam energies. The results of such calculations directly yield the spatially dependent source functions that dictate and control *e*-beam-induced conductivity within the diamond switches. A detailed evaluation of the source function is essential and important since it constitutes an important input parameter for subsequent drift-diffusion calculations of the overall electrical characteristics. Furthermore, in order for the switch to have an optimum power gain, it is critical for the *e*-beam penetration not to exceed the thickness of the diamond film. Hence, it becomes necessary to evaluate the energy-dependent penetration depths and use the results to adequately predict and select material thicknesses.

In the following sections we begin by briefly outlining the Monte Carlo numerical scheme on which the electron penetration range and excess carrier-generation profile calculations are based. A description of the *e*-beam setup and the relevant experimental details is subsequently given. The results are then presented with adequate comparisons between experimental data and theoretical simulations. This

 0021-8979/93/74(3)/1568/7/$6.00

is followed by concluding remarks relevant to e-beam-induced switching in diamond.

II. MONTE CARLO SIMULATION

Our simulations to study the energy-dependent e-beam penetration in diamond and the subsequent formation of excess carriers have been based on the numerical Monte Carlo procedure.[16,17] This probabilistic technique provides a microscopic evaluation of the spatial interactions between electrons and the constituent target atoms, and keeps track of the trajectories of individual electrons in phase space. Multiple scattering, inelastic energy losses, and momentum randomization are all taken into account as a result. In the present simulations, elastic scattering has been treated on the basis of a screened Coulomb potential $V(r)$ of the form[4] $V(r)=(Ze^2/r)\exp[-(r/a)]$, with Z being the target atomic number, r the radial electronic distance from the target nucleus, and a representing an effective screening length. This screening parameter is given in terms of the Bohr radius a_0 as $a=a_0Z^{-1/3}$ and is based on the Wentzel model.[4] For greater rigor, perhaps, one could conceivably have used a multiexponential screening function,[18] or taken a Lenz-type approach,[19] instead. However, as will become apparent from our numerical results, the Wentzel approximation is quite adequate and clearly suffices for the present calculations. Within the Born approximation, the above then yields the following energy-dependent Rutherford-type differential cross section $d\sigma(\theta)$:[8]

$$\frac{d\sigma(\theta)}{d\theta}=\frac{e^4Z^2\pi\sin(\theta)d\theta}{8(4\pi\epsilon E)^2[\sin^2(\theta/2)+\delta]^2}, \tag{1}$$

where $\delta=3.4\times10^{-3}Z^{2/3}E^{-1}$, and E is the electron energy in keV. Integrating Eq. (1) over all possible scattering angles from 0 to π leads to the following energy-dependent elastic scattering cross section $\sigma_{el}(E)$:

$$\sigma_{el}(E)=\frac{e^4Z^2\pi}{4(4\pi\epsilon E)^2\delta(1+\delta)}. \tag{2}$$

This elastic scattering cross section is used within our Monte Carlo formulation to compute the energy-dependent mean free paths for each of the simulated electrons. It may be noted that the above formulation for elastic scattering is valid and remains reasonably accurate provided the incident electron energies are not too small and that the atomic numbers of the target material are not too large. Previous studies have indicated that the Rutherford cross sections cease to be adequate roughly for energies below 20 keV and atomic numbers above silicon.[8] Fortunately, both of the above requirements are easily satisfied in the present case. The target diamond has an atomic number well below that of silicon, while the typical electron energies being investigated here have sufficiently high values ranging from 90 to 160 keV. As a result, we avoid having to use cumbersome partial-wave methods or Mott–Massey-type formulations,[20] which do not yield analytical closed-form expressions. Based on the scattering cross section of Eq. (1), the angular probability distribution function required for selection of the angles after every elastic scattering event can easily be evaluated. The requisite normalized expression $P(\theta)$ works out to

$$P(\theta)=(1+\delta)\left(1-\frac{2\delta}{1-\cos(\theta)+2\delta}\right). \tag{3}$$

We have used the well-known Bethe expression for energy loss[21] to treat inelastic scattering of electrons for the present work. Utilization of such a continuous energy loss approximation has previously been known to yield acceptable results for a variety of situations, and hence the same scheme is adopted here. Accordingly, the energy loss per unit distance dE/ds is given by

$$\frac{dE}{ds}=-7.85\times10^4\frac{Z\rho}{AE}\log\left(\frac{1.166E}{J}\right)\ \text{keV/cm}, \tag{4}$$

where ρ is the density of the target material, A is the atomic weight, E the electronic energy in keV, and J the mean ionization potential[22] given as $J=(9.76\,Z+58.5\,Z^{-0.19})$ eV.

The Monte Carlo simulations have been carried out by following the individual trajectories of 8000 primary electrons incident normally (i.e., parallel to the z axis) on the diamond sample at energies E_i. Only the electrostatic processes discussed above were taken into account, and possible magnetic interactions[23] between electrons and atomic nuclei ignored. The path lengths were assumed to follow Poisson-type distribution, and the step length Δs was computed using Eq. (2) according to $\Delta s=-A(\sigma_{el}N_A\rho)^{-1}\ln(R_1)$, with N_A being the Avogadro number and R_1 a normalized random number generated within the simulation program. The corresponding energy loss ΔE was computed for each segment of the trajectory Δs based on Eq. (4) as $\Delta E=\Delta s(dE/ds)$. This numerical value of ΔE over each segment was subsequently used to compute the internal electron-hole generation density (or source function) at the corresponding spatial grid point. It was assumed that the energy E_{eh} necessary to create an electron-hole pair by an incident electron is typically 3.1 times the band gap E_{gap}.[24] The source function N_{eh} at each grid point was therefore given as $N_{eh}=\Delta E\,(3.1\,E_{gap})^{-1}$. It may be noted in this regard that the use of such an empirical relation for N_{eh} is not arbitrary, but instead is well justified on experimental grounds.[24]

The polar angle for elastic scattering denoting a deflection through θ was evaluated from Eq. (3). Using a second random number R_2, this computation was performed as

$$\theta=\cos^{-1}[1-(2\delta R_2)/(1+\delta-R_2)].$$

Due to azimuthal symmetry, the azimuthal angle ϕ was randomly distributed between 0 and 2π. The new direction θ_z'' for subsequent electronic motion relative to the z axis could then be obtained in terms of the deflecting angles θ and ϕ. The final expression works out to

$$\theta_z''=\cos^{-1}[\cos(\theta_z)\cos(\theta)+\sin(\theta_z)\sin(\theta)\cos(\phi)],$$

with this new angle θ_z'' being used to replace the previous value θ_z after every elastic scattering event. Finally, the

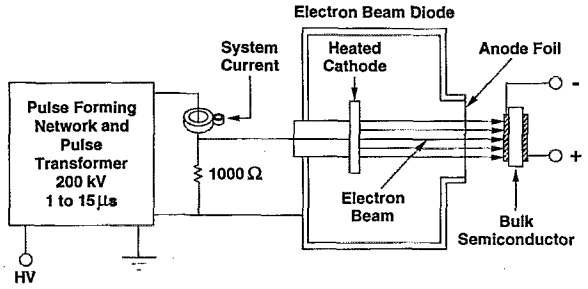

FIG. 1. Schematic representation of the electrical circuit used for electron-beam generation. Energies of up to 190 keV were attainable as a result.

Monte Carlo procedure was terminated for each electron after its energy had been reduced below the mean ionization potential J defined in Eq. (4).

III. EXPERIMENTAL DETAILS

The electron-beam system discussed in detail elsewhere[11] consisted of a pulsed thermionic diode, its vacuum chamber, and a pulse-forming network (PFN) as shown schematically in Fig. 1. The 15 segment PFN consisted of a 3.4 μH inductor and two 24.5 nF capacitors in parallel per stage, and was charged through a 3 MΩ resistor by a dc power supply having a 40 kV rating. A high-voltage diode was used in series with the charging line to eliminate reflections due to possible mismatch. The charging system was discharged through a nitrogen spark gap operated at pressures between 1 and 10 psi, and was triggered by a pulse from an ignitron-type electrode. The PFN output was through a 1:11 step-up transformer into a matched load (1000 Ω). The system was capable of delivering a variable pulse ranging from 1 to 15 μs, and was used to accelerate electrons emitted from a thermionic diode. The energy of the liberated electrons could be varied from 100 to 190 keV, with current densities up to 35 mA/cm^2. The cathode used for thermionic emission consisted of tungsten filaments surrounded by a grid enclosure which served as a corona shield. The anode was a 1 mil titanium foil grounded to the system chamber. As a result of this foil, which constituted the anode, the energy distribution of the emergent electron beam could not be monochromatic. Instead both statistical deviations in the traversal paths and the energy losses occurring due to inelastic collisions within the foil should affect the final distribution profile. Hence, for purposes of accurate simulation and accurate representation of the actual experimental conditions, this detail had to be adequately considered. We shall return to a discussion of this issue later, and quantitatively demonstrate the consequence through Monte Carlo simulations.

The electron flux emerging from the 35 μm diamond target was collected by a graphite Faraday cup. Graphite was chosen as the collector material because of its high conductivity and low secondary electron emission coefficient. By recording the intensity of the collected current density, a direct measure of the fractional transmission was

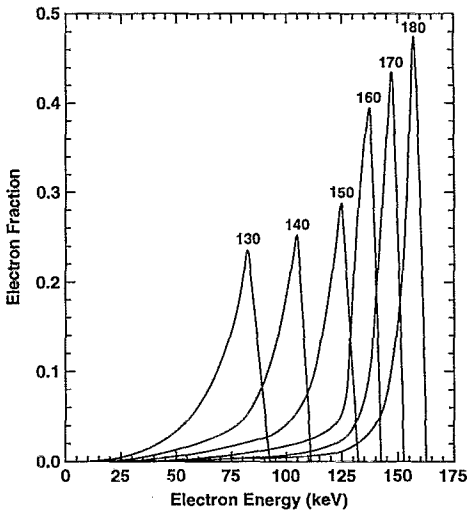

FIG. 2. Monte Carlo simulation results showing energy distributions after the traversal of monoenergetic electron beams through a 1 mil titanium foil. The set of curves correspond to incident electron energies ranging from 120 through 180 keV.

obtainable. Such information is related to the energy loss processes within the diamond, and indirectly reflects the stopping power. Finally, the experimental measurements also provided the means to appropriately determine the energy threshold for electron-beam penetration through the sample for a given thickness.

IV. RESULTS AND DISCUSSION

Monte Carlo simulations were performed to analyze e-beam penetration and excess carrier generation within a 35 μm diamond sample for the experimental setup of Fig. 1. Presence of the 1 mil titanium foil which served as the anode was explicitly taken into account. This involved initial calculations of the energy distribution function for the emergent electron beam after its passage through the Ti foil. The results are shown in Fig. 2, and represent both energy loss due to inelastic scattering within the foil and a statistical diffusion in energy space. The electronic energies prior to incidence were monochromatic, and ranged from 120 to 180 keV as shown. The relative heights of the curves denote the fractional transmitted flux, which clearly increases with the accelerating potential as expected. Also, not surprisingly, the smearing of the energy distribution after transmittance is seen to be larger for lower incident energies since the strength of the inelastic scattering gets stronger as the energy is decreased. The curves shown in Fig. 2 were then fit to analytical fourth-order polynomials in order to obtain an analytical closed-form expression of the energy distribution for simulations involving the 35 μm diamond sample.

Based on the numerical Monte Carlo procedure already discussed, simulations were performed to compute the fractional electron flux transmitted through the diamond target, based on energy distributions obtained from the previous results of Fig. 2. Such calculations represent penetration of the electrons through the diamond film as a

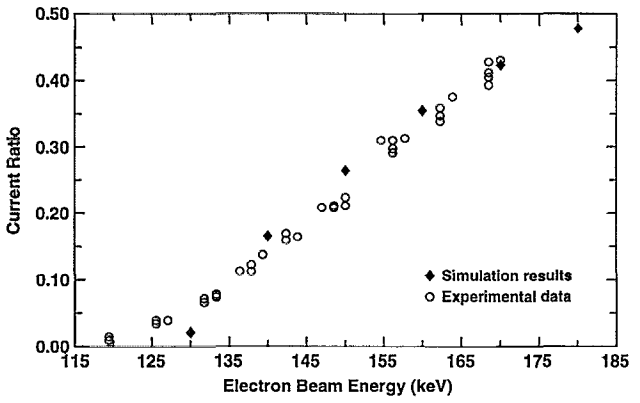

FIG. 3. Experimental data and Monte Carlo results showing the energy-dependent penetration of incident electrons through a 35 μm diamond sample. The two sets of values of the fractional transmittance are in very good agreement.

function of the applied accelerating potential. The primary objective was to compare the predictions of the theoretical model with measured values of the factional transmittance. The latter was experimentally determined by placing two Faraday cups within the sample test chamber. One of them was placed directly behind the diamond sample, while the second cup which served as a reference was held in place without any diamond target in front. As a result, it was possible to directly record ratios of the electron flux penetrating the diamond sample, as a function of the incident electron-beam energy. Our results, both experimental and theoretical, are shown in Fig. 3. The scattered circles represent experimental data points, while the dark points are the values obtained from Monte Carlo calculations. The agreement between theory and actual experiment is obviously very good, and hence lends strong credence to our simulation scheme. A number of features are immediately apparent from the figure. First, there exists an energy threshold of about 125 keV for penetration of the electron beam into the 35 μm diamond. Below this energy value, the intensity of the collected current is quite negligible. The Monte Carlo simulations are in agreement on this issue. Next, the transmitted flux does not exhibit a dramatic increase with energy, nor does it quickly saturate. This is a result of a smeared energy distribution created by the Ti foil, and is also due to the finite size of the sample. Contributions from the low-energy electronic population of the incident beam offset the role of the high-energy particles, and vice versa. Consequently there is a collective internal averaging effect, and hence the output does not exhibit a sharp structure or any dramatic increases. A similar outcome arises from the finite dimensions of the sample. Not all of the particles having energies above the threshold can be collected by the Faraday cup due to the lateral movement of electrons within the sample. Such lateral velocity components are created by the internal elastic scattering, which is particularly strong at the lower energies in accord with Eq. (3). Hence, the collected current does not exhibit a particularly high value.

Simulations of the energy-dependent electron range and the average e-beam penetration normal to the plane of incidence were carried out for a range of electron energies. The electron-beam energy was assumed to be monoenergetic ranging between 30 and 180 kV and the Ti foil was ignored. Based on the close agreement between the numerical values and the measured data of Fig. 3, we believe that our Monte Carlo calculations of the average path length $L_{\text{avg}}(E)$ and the normal e-beam penetration depth $L^z_{\text{avg}}(E)$ yield accurate and correct predictions. Such information regarding the two parameters L_{avg} and L^z_{avg} is important, since it fixes an upper limit in selecting the incident e-beam energies that can optimize the operation of a given diamond switch. For example, the overall efficiency of a diamond switch would obviously be reduced if an e-beam energy value was chosen for which the corresponding penetration depth $L^z_{\text{avg}}(E)$ far exceeded the sample thickness itself. The requisite computations of the average path length $L_{\text{avg}}(E)$ can easily be performed through numerical integrations of the Bethe equation (4). Analytical expressions for the energy-dependent range have been obtained in the literature by curve fitting the results of numerical integrations. In keeping with experimental data, equations for the total path length $L_{\text{avg}}(E)$ are usually expressed by a power law of the form $L_{\text{avg}}(E)=KE^n$, with the parameter K and the exponent n being material-dependent constants.[25,26] However, information regarding the normal penetration depth $L^z_{\text{avg}}(E)$, cannot be obtained analytically through simple integrations as is possible with $L_{\text{avg}}(E)$, cannot be obtained analytically through simple integrations as is possible with $L_{\text{avg}}(z)$. Instead the statistical nature of the random energy-dependent collisions, and the angular deflections have to be carefully taken into account for calculations of $L^z_{\text{avg}}(E)$. Such a task, therefore, can ideally and easily be performed through Monte Carlo-type simulations. Since, as already stated, the penetration $L^z_{\text{avg}}(z)$ constitutes an important parameter for the e-beam-controlled switch, the necessary energy-range simulations were performed in this study. To the best of our knowledge such calculations have not been carried out previously for diamond material.

The energy dependence of the total path length and the normal penetration depth of electrons in diamond, as obtained from Monte Carlo simulations, is shown in Fig. 4. The dashed line corresponds to a previous empirical power-law relation,[27] while the best-fit lines through the two sets of data points correspond to the Monte Carlo simulations. The empirical expression for the range $L(E)$ used here for comparison was given by $L=4.28\times10^{1.75}E^{1.75}/\rho$, with ρ being the density of diamond. The present results are again seen to be in good agreement with past estimates. Also as evident from the figure, the total path lengths traversed by the particles turn out to be roughly twice as long as their perpendicular penetration, and the ratio is nearly constant throughout the entire energy interval. Using a power law, the calculated data set yielded a reasonably good fit to the following analytical expressions:

$$L_{\text{avg}}(E)=0.0203E^{1.702}$$

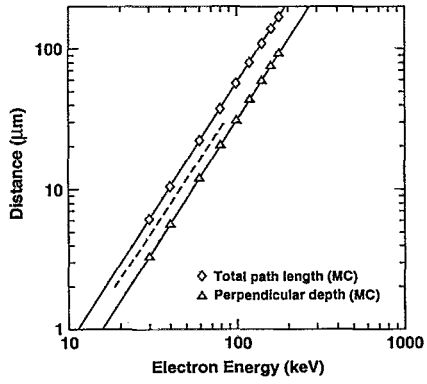

FIG. 4. Monte Carlo calculations of the energy-dependent electron-beam penetration into diamond. Data points for the average path length $L_{avg}(E)$ and perpendicular depth $L^z_{avg}(E)$ are shown as a function of the incident electron energy with best fit lines through them. The dashed line represents an empirical relation (see Ref. 27).

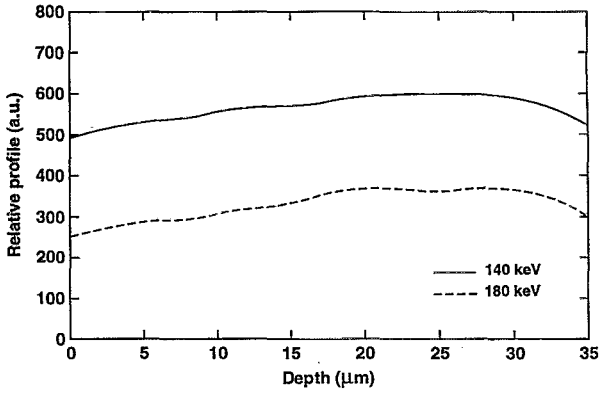

FIG. 5. Relative profiles of excess carrier generation within diamond for accelerating potentials of 140 and 180 keV. The results were obtained from Monte Carlo simulations and included the 1 mil Ti foil.

and

$$L^z_{avg}(E) = 0.010\,76E^{1.705}, \tag{5}$$

with E being the incident electron energy in keV and both distances being expressed in micrometers. Figure 4 reveals that a slightly higher value of the exponent would result if only the data points lying below 100 keV were to be considered. Such minor changes in the power-law coefficients with energy are a result of the nonlinear Bethe law and have been seen in other material as well.[25] Finally, we note that an exponent value larger than 1.702 as indicated by the present study for energies below 100 keV compares very favorably with a previous estimate of 1.725 obtained for the 5–80 keV interval.[27]

Simulations of the e-beam-induced free-carrier generation in diamond were carried out next, with both a monoenergetic electron beam and the electron beam passing through the Ti foil. Given the excellent agreement between theoretical predictions and the experimental data of Fig. 3, we once again expect the Monte Carlo generated internal carrier profiles to be quite accurate and reliable. The primary objective in carrying out the simulations was to examine the impact of the incident e-beam energy on the shape and relative intensity of the resulting internal free-carrier profiles. Such details are important to the eventual operation of the diamond switch, since the profiles dictate the drift and diffusive flow of charge within the system. The internal source function also directly affects localized trap filling, creation of inhomogeneous space charge within the sample, and the shaping of electric-field profiles that control charge movement.[28] Results from our simulations are given in Fig. 5. The curves represented the relative free-carrier generation profiles for 180 and 140 keV e-beam accelerating potentials. The behavior seen can be easily understood in terms of the energy-dependent inelastic scattering which is governed by the Bethe equation (4). The energy loss per unit path length monotonically increases with reductions in the electron energy, and can become very large at the lowest values. Consequently, the source function is higher for the 140 keV situation, as compared to the 180 keV potential. Furthermore, since both the two energies are sufficiently large for penetration of the 35 μm diamond, the profile does not show any significant structure. A more pronounced peak or local maxima could have resulted, however, in case the incident electrons had been completely stopped within the sample. Such a situation would have led to large energy losses over localized spatial regions deep into the material, with concomitant increases in the source function away from the front face.

Finally, feasibility studies of tailoring the internal carrier profiles and source functions were carried out through Monte Carlo simulations. Since in practice the samples can be expected to have nonuniform trap distributions leading to undesirable inhomogeneous internal electric fields, it would be advantageous to attempt controlling the switch performance through appropriate tailoring of the generation function. A possible method of so doing could be based upon suitable variations and shaping of the incident e-beam energy distribution. The disadvantage, however, would be in terms of the additional dissipative losses within the metallic foils that may be used to shape the energy distributions. Although the practical implementation is perhaps not as simple, we explore and demonstrate the possibility here for completeness and examine the possible effects that can be expected. Taking a 130 keV accelerating potential, the simulation results obtained for monoenergetic and distributed incident electron beams (as obtained by passing through the Ti foil) are shown in Fig. 6. Not surprisingly, with monoenergetic electrons the spatial variations are not very pronounced since most of the incoming electrons can pass through the *entire* sample. A slight bump occurs however, at around 27 μm into the sample, and is a result of relatively large inelastic scattering at low energies. Although the energy losses are expected to be still higher toward the very end of the sample, the overall generation function does not attain as high a value. This is primarily a result of elastic scattering which limits the population of surviving electrons that is able to penetrate and reach deep into the sample. The influence of the larger energy losses with distance is partially offset as a result.

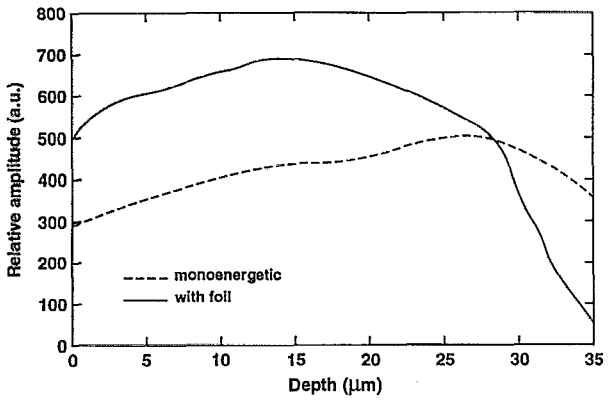

FIG. 6. Monte Carlo results demonstrating the ability to tailor the internal spatial distribution of the generated carriers. One of the curves corresponds to a monoenergetic 130 keV incident beam, while the other used the distribution of Fig. 2 for a 130 keV accelerating potential.

With a distribution of energies, on the other hand, the source function has a larger value, and exhibits a nonuniform profile due to contributions from the low-energy electrons. The free-carrier enhancements over the initial portions of the diamond sample reflect the larger energy loss in accordance with the Bethe formulation, and hence is similar to the results of Fig. 5. The values sharply decline beyond 30 μm, and denote the inability of the low-energy electrons to penetrate through the entire sample.

Based on the results, one can expect important consequences for electrical transport within the diamond sample. The first and obvious impact would be on the diffusion current components due to changes in the concentration gradients, and would affect the initial transient response during the switching process. Furthermore, under an externally applied field, the diffusive component would work to enhance the drift component for one polarity setting, and impede net charge transfer for the reversed biasing. Such an affect on the electrical characteristics has already been observed for asymmetrical diamond structures.[12] Next, the transient trap-filling dynamics would also be different as a result of the dissimilar source functions. This in itself has important implications. First, due to the lower-generation values with the monoenergetic electron beam, the switch currents would be slightly lower during the on state of the switch. Second, the trap-filling process would take a slightly longer time period, and would depend more on current injection from the contacts as compared to the situation involving a distribution of incident electron energies. Finally, due to the lower asymmetry associated with the monoenergetic beam, control of current transport through the use of Schottky or noninjecting contacts would be less difficult. With higher asymmetry in the profiles, on the other hand, one can expect larger nonuniformities in the electric fields.[29] This could possibly lead to unwanted injection at the contacts due to a combination of field-enhanced tunneling, Schottky barrier lowering, and hot-carrier thermionic emission. As a result, the utility of having blocking contacts might be unacceptably impaired.

V. CONCLUSIONS

Experimental studies and theoretical simulations of electron-beam penetration and free-carrier generation in natural diamond have been conducted. The primary objective was to investigate the potential of electron beams as efficient sources for ionizing insulating materials for high-power repetitive switching applications. Experiments were carried out to directly obtain data on the energy-dependent transmission of e beams into 35 μm diamond. Such results are important since they relate to optimization of the e-beam-controlled switch efficiency and power gain. The expected change inconductance, current swing, and the internal space-charge development dynamics are also dictated by the e-beam-induced excess-carrier distribution. The details delicately depend upon a variety of factors including the input flux, energy distribution of the incident electron swarm, and the thickness of the target sample. In order to better understand the role and influence of all the above factors, numerical Monte Carlo simulations were performed in addition to the experiments.

Our results reveal that a threshold energy of about 125 keV is necessary for complete penetration into a 35 μm diamond sample. This represents a lower bound on the power input if complete bulk ionization is required. The spatial distribution of the source function, however, is not very uniform in such a case. The uniformity can be improved by using higher energies, but system efficiency is likely to suffer and the internal bulk ionization levels would also decrease. The latter is a direct consequence of the inelastic energy-loss function which decreases at higher energies. The Monte Carlo simulations yielded very good agreement with actual experimental data, and were used to analyze the probe both the internal spatially dependent source functions and the energy-dependent e-beam penetration ranges. Our simulation results indicate that both the total path length and the perpendicular penetration distance of the electrons in diamond could be adequately represented by a simple power law. The exponent had a value of about 1.7 and compares well with the existing power laws. The ratio between the total path length and the perpendicular penetration depth from the surface was seen to be nearly independent to the incident particle energy for the 30–180 keV range.

Our results also clearly demonstrate the feasibility of tailoring the excess carrier generation, and hence could be used to advantage in optimizing the electrical response of the overall electron-beam-controlled switch. Quite obviously, such tailoring may be required for samples having nonuniform impurity and trap distributions. Finally, based on our simulation results, we find that the choice of the energy distribution of the incoming electrons critically affects the internal electric-field distribution, and hence can play an important role in current injection at the contacts.

ACKNOWLEDGMENTS

The authors acknowledge and thank L. S. Pan and J. D. Kania (Lawrence Livermore Laboratory) for helpful discussions, and M. K. Kennedy (Old Dominion Univer-

sity) for technical assistance. This work was supported by a grant from DoE through the Lawrence Livermore National Laboratory.

[1] H. M. Terril, Phys. Rev. **22**, 101 (1923); N. F. Mott, Proc. R. Soc. London Ser. A **124**, 425 (1929).
[2] H. Bethe, Ann. Phys. (Leipzig) **5**, 325 (1930); **87**, 55 (1928).
[3] H. Niedrig, J. Appl. Phys. **53**, R15 (1982), and references therein.
[4] For example, G. Wentzel, Z. Phys. **40**, 590 (1927).
[5] S. Goudsmit and J. L. Sauderson, Phys. Rev. **57**, 24 (1940).
[6] T. E. Everhart, J. Appl. Phys. **31**, 1483 (1960); W. S. McAfee, *ibid.* **47**, 1179 (1976).
[7] L. Pensak, Phys. Rev. **75**, 472 (1949); K. G. McKay, Phys. Rev. **74**, 1606 (1948).
[8] D. B. Holt and D. C. Joy, *SEM Microcharacterization of Semiconductors* (Academic, London, 1989); L. Reimer, *Scanning Electron Microscopy: Physics of Image Formation and Microanalysis* (Springer, Berlin, 1985).
[9] See, for example, Special Issue on Power Modulators, IEEE Trans. Electron Devices **ED-38**, 685 (1991); G. Schaefer and K. H. Schoenbach, IEEE Trans. Plasma Sci. **PS-14**, 561 (1986).
[10] A. V. Brown, IEEE Trans. Electron Devices **ED-10**, 8 (1963), and references therein.
[11] R. P. Brinkmann, K. H. Schoenbach, D. C. Stoudt, V. K. Lakdawala, G. Gerdin, and M. K. Kennedy, IEEE Trans. Electron Devices **ED-38**, 701 (1991); D. C. Stoudt, K. H. Schoenbach, R. P. Brinkmann, V. K. Lakdawala, and G. A. Gerdin, *ibid.* **ED-37**, 2478 (1990).
[12] R. P. Joshi, M. K. Kennedy, K. H. Schoenbach, and W. W. Hofer, J. Appl. Phys. **72**, 4781 (1992).
[13] R. A. Rudder, G. C. Hudson, J. B. Posthill, R. E. Thomas, and R. J. Markunas, Appl. Phys. Lett. **59**, 791 (1991); K. V. Ravi and C. A. Koch, *ibid.* **57**, 348 (1990).
[14] D. E. Meyer, R. O. Dillon, and J. A. Wollman, J. Vac. Sci. Technol. A **7**, 2325 (1989); K. Kurihara, K. Sasaki, M. Kawarada, and N. Koshiro, Appl. Phys. Lett. **52**, 437 (1988).
[15] M. W. Geis, Mater. Res. Soc. Symp. Proc. **162**, 15 (1990).
[16] A. Jablonski, Surf. Interface Anal. **14**, 659 (1989), and references therein; D. C. Joy, J. Microsc. **147**, 51 (1987); M. Dapor, Phys. Rev. B **46**, 618 (1992).
[17] K. Murata, D. F. Kyser, and C. H. Ting, J. Appl. Phys. **52**, 4396 (1981); D. E. Newbury, H. Yakowitz, and R. L. Myklebust, Appl. Phys. Lett. **23**, 448 (1973).
[18] H. L. Cox and R. A. Bonham, J. Chem. Phys. **47**, 2599 (1967).
[19] F. Lenz, Z. Naturforsch A **9**, 185 (1954).
[20] N. F. Mott and H. S. W. Massey, *The Theory of Atomic Collisions* (Oxford University Press, Oxford, 1965).
[21] H. Bethe, *Handbook of Physics* (Springer, Berlin, 1933), Vol. 24, p. 273.
[22] M. J. Berger and S. M. Seltzer, National Research Council Publication 1133, Washington D. C., 1964, p. 205.
[23] J. Kessler, in *Polarized Electrons* (Springer, Berlin, 1976), Chap. 3.
[24] C. A. Klein, J. Appl. Phys. **39**, 2029 (1968).
[25] J. R. Young, J. Appl. Phys. **27**, 1 (1956); R. O. Lane and D. J. Zaffarano, Phys. Rev. **94**, 916 (1954); W. F. Libby, Anal. Chem. **19**, 2 (1947).
[26] T. E. Everhart and P. H. Hoff, J. Appl. Phys. **42**, 5837 (1971); K. Kanaya and S. Okayama, J. Phys. D **5**, 43 (1972).
[27] H. J. Leamy, J. Appl. Phys. **53**, R51 (1982).
[28] P. Mark and M. A. Lampert, in *Current Injection in Solids* (Academic, New York, 1970).
[29] S. E. Ralph and D. Grischkowsky, Appl. Phys. Lett. **59**, 1972 (1991).